Effective Reconstruction Approaches to Millimeter-Wave Imaging of Humans

J. Detlefsen, A. Dallinger, S. Huber, S. Schelkshorn

Technische Universität München
Lehrstuhl für Hochfrequenztechnik
Fachgebiet Hochfrequente Felder und Schaltungen

ABSTRACT
Increasing demands for screening personnel for concealed objects lead to additional research efforts related to suitable imaging systems and their industrial realization. In this context millimeter-wave systems are a promising approach, because the radiation does not present a health hazard to people under surveillance and readily passes through many optically opaque materials such as clothing fabrics allowing for the identification of concealed objects. Due to the extent of the human's body and the resultant required amount of 3D resolution cells with a magnitude of 15 mm or less, in principle all existing and proposed systems have to deal with a huge amount of scattering data which have to be acquired and processed. For a highly resolved image principally as much information as available should be used. This means that the scattered field principally has to be measured across extended 2D surfaces surrounding the object and for a frequency band which is as large as possible. The practical limitations come from the implementation of the system and are related to the hardware expense [1, 2] for the imaging setup and to the required acquisition time.

1 INTRODUCTION

Imaging configurations which have led to experimental systems measure field distributions either in the focal plane of a lens or mirror or are of holographic type, which requires that the total scattered field including phase information has to be captured. Within first approach reconstruction is done by the lens or mirror which saves most of the extreme computational effort necessary to reconstruct the image from the holographic field. As the first approach is less flexible with respect to focusing the paper will concentrate on processing required for the holographic case. The general holographic imaging approach can be characterized by the requirement of computer-aided reconstruction of the 3D distribution of scattering centers from the scattered field, typically measured in a monostatic configuration along a part of the surface surrounding the object or at a specific distance from the object. The surface can be according to the selected measurement configuration of different type, e.g. of planar, cylindrical or spherical shape. In all cases the scattered field can be obtained principally across a 2D surface patch. The field can be acquired in parallel by hardware using a suitably located array of transmit and receive-modules or by scanning one or a few modules across the surface of interest generating a so-called synthetic aperture. As the application in our case is to image person at close distance of a meter or less a cylindrical surface is the appropriate measurement surface, while the object is characterized on a cartesian grid.

2 GENERAL THEORY OF RECONSTRUCTION

2.1 Description of Measurement Aperture and Object

Fig. 1 shows the cylindrical aperture and the object. The aperture sampling grid and the object coordinates are defined by $\boldsymbol{r}_\mathrm{a} = (x_\mathrm{a}, y_\mathrm{a}, z_\mathrm{a})^\top = (\rho_\mathrm{a}\cos\varphi_\mathrm{a}, \rho_\mathrm{a}\sin\varphi_\mathrm{a}, z_\mathrm{a})^\top$ and $\boldsymbol{r}_\mathrm{o} = (x_\mathrm{o}, y_\mathrm{o}, z_\mathrm{o})^\top$ ($|\boldsymbol{r}_\mathrm{o}| \leq D$, with D the object dimensions), respectively, with ρ_a being the aperture radius. In the experimental setup the cylindrical aperture data are synthesized by moving a sensor to each of the required locations creating a synthetic aperture. The angular variable φ_a describes the rotation of the sensor around the object. The variable z_a stands for the linear aperture in z-direction. The cylindrical aperture's extend is limited by $\varphi_\mathrm{a} = \varphi_{\mathrm{a,min}} \ldots \varphi_{\mathrm{a,max}}$ and $z_\mathrm{a} = z_{\mathrm{a,min}} \ldots z_{\mathrm{a,max}}$. The apertures lengths in both directions are determined by L_{φ_a} and L_{z_a}.

2.2 Helmholtz Wave Equation, Free Space Green's Function and Wave Expansion of Point Source

Considering time harmonic fields the scalar Helmholtz wave equation satisfies Maxwell equations at every spatial observation point $\boldsymbol{r}$. A general form may be written as

$$\left(\Delta + k_0^2\right) u(\boldsymbol{r}) = -q(\boldsymbol{r}) \tag{1}$$

where $u(\boldsymbol{r})$ describes some arbitrary field component, k_0 the wavenumber in free space and $q(\boldsymbol{r})$ some source distribution originating from an exciting field [3]. Considering Dirac-like excitations, i.e. $q(\boldsymbol{r}) = \delta(\boldsymbol{r})$ a solution of (1) is the free

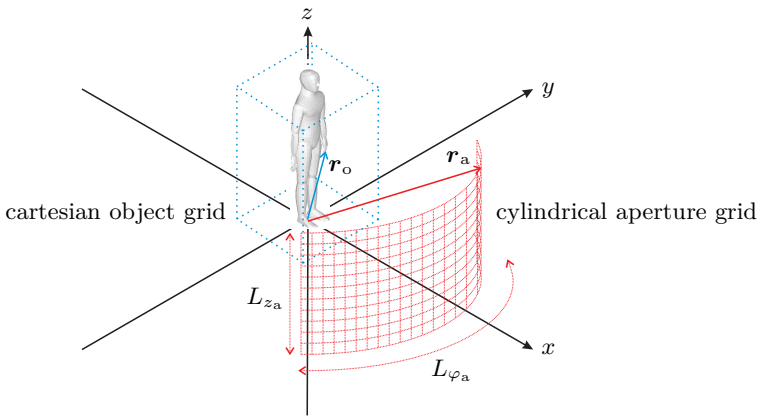

Fig. 1: geometrical setup: the cylindrical aperture grid is defined by the vector $\boldsymbol{r}_\mathrm{a}$, the cartesian object grid is determined by $\boldsymbol{r}_\mathrm{o}$

space Green's function $g(\boldsymbol{r}) = e^{-j\boldsymbol{kr}}/(4\pi|\boldsymbol{r}|)$. The Helmholtz wave equation can be transformed into its spatial spectral domain which gives

$$\left(-\boldsymbol{k}^2 + {k_0}^2\right) u(\boldsymbol{k}) = -q(\boldsymbol{k}) \quad . \tag{2}$$

The homogeneous solution, i.e. $q(\boldsymbol{k}) = 0$ but $u(\boldsymbol{k}) \neq 0$ requires the dependency between the background wavenumber k_0 and the spatial spectral domain vector to be $\boldsymbol{k}^2 = {k_0}^2 = {k_x}^2 + {k_y}^2 + {k_z}^2$. Using (2), assuming an exciting point source, i.e. $q(\boldsymbol{k}) = 1$ and applying the shift operation in Fourier domain, a spectral domain equivalent of the Green's function of a point source can be found to be [4]

$$g(\boldsymbol{r}, \boldsymbol{r}') = \frac{e^{-j\boldsymbol{k}(\boldsymbol{r}-\boldsymbol{r}')}}{4\pi|\boldsymbol{r}-\boldsymbol{r}'|} = \frac{-1}{(2\pi)^3} \iiint\limits_{\boldsymbol{k}} \frac{e^{-j[k_x(x-x')+k_y(y-y')+k_z(z-z')]}}{k^2 - {k_x}^2 - {k_y}^2 - {k_z}^2} \,\mathrm{d}k_x \,\mathrm{d}k_y \,\mathrm{d}k_z \tag{3}$$

2.3 Linearized Inverse Scattering

Basically, imaging penetrable objects means solving for an unknown local inhomogeneous distribution of $k(\boldsymbol{r})$ when only the incident field u_i and the scattered field u_s are known ($u = u_\mathrm{i} + u_\mathrm{s}$). The local inhomogeneous scatterer characteristics can also be defined as a spatially dependent object- or contrast function $o(\boldsymbol{r}) = k(\boldsymbol{r})^2 - {k_0}^2$. By using the Born or weak scatterer approximation, i.e. $u_\mathrm{s} \ll u_\mathrm{i}$ and $o(\boldsymbol{r}) \ll 1$ the non-linear inverse scattering equation (Lippmann-Schwinger integral equation [5]) can be linearized and a numerically useful solution applicable to the so-called linearized inverse scatting problem can be found as follows

$$u_\mathrm{s}(\boldsymbol{r}_\mathrm{a}) = \iiint\limits_{|\boldsymbol{r}_\mathrm{o}| \leq D} o(\boldsymbol{r}_\mathrm{o}) u_\mathrm{i}(\boldsymbol{r}_\mathrm{o}) g(\boldsymbol{r}_\mathrm{a}, \boldsymbol{r}_\mathrm{o}) \,\mathrm{d}\boldsymbol{r}_\mathrm{o} \quad , \mathrm{d}\boldsymbol{r}_\mathrm{o} = \mathrm{d}x_\mathrm{o} \,\mathrm{d}y_\mathrm{o} \,\mathrm{d}z_\mathrm{o} \quad . \tag{4}$$

which means that the scattered field u_s at the observation point $\boldsymbol{r}_\mathrm{a}$ is just a linear summation of the object function $o(\boldsymbol{r})$ excited by the incident field and weighted by the Green's function $g(\boldsymbol{r}_\mathrm{a}, \boldsymbol{r}_\mathrm{o})$.

Equation (4) can be expanded to also handle monostatic and quasi monostatic radar setups by applying the so-called radiating or exploding reflector model. There the excited object function $o(\boldsymbol{r})u_\mathrm{i}$ acts like point scatterers radiating synchronous with a propagation speed half the propagation speed of the background medium, i.e. $c = c_0/2$ and $k = 2k_0$. This leads to an expression for the modified scattered field

$$u_\mathrm{s}(\boldsymbol{r}_\mathrm{a}) = \iiint\limits_{|\boldsymbol{r}_\mathrm{o}| \leq D} o(\boldsymbol{r}_\mathrm{o}) g(\boldsymbol{r}_\mathrm{a}, \boldsymbol{r}_\mathrm{o}) \,\mathrm{d}\boldsymbol{r}_\mathrm{o} \quad . \tag{5}$$

3 3D CYLINDRICAL RECONSTRUCTION ALGORITHM

3.1 Derivation of the algorithm

To properly represent the data obtained by our experimental setup we use polar cylindrical aperture coordinates $(\rho_\mathrm{a}, \varphi_\mathrm{a}, z_\mathrm{a})$. Starting from 5 and using 3 we obtain

$$u_s(\varphi_\mathrm{a}, z_\mathrm{a}, \omega) = \frac{-1}{(2\pi)^3} \iiint\limits_{|\boldsymbol{r}_\mathrm{o}| < D} o(\boldsymbol{r}_\mathrm{o}) \iiint\limits_{\boldsymbol{k}} \frac{e^{-j[k_x(x_\mathrm{a}-x_\mathrm{o})+k_y(y_\mathrm{a}-y_\mathrm{o})+k_z(z_\mathrm{a}-z_\mathrm{o})]}}{4k^2 - k_x^2 - k_y^2 - k_z^2} \,\mathrm{d}k_x \,\mathrm{d}k_y \,\mathrm{d}k_z \,\mathrm{d}x_\mathrm{o} \,\mathrm{d}y_\mathrm{o} \,\mathrm{d}z_\mathrm{o} \quad . \tag{6}$$

The spectral variables k_x, k_y and k_z represent the wave vectors on a cartesian grid, which can be substituted by polar cylindrical coordinates (k_r, Φ, k_z) for the spectral domain, i.e. $k_x = k_r \cos\Phi$ and $k_y = k_r \sin\Phi$ with $k_r = \sqrt{k_x^2 + k_y^2}$

and $\Phi = \arctan(k_y/k_x)$. In our further derivation we generally will neglect all amplitude terms because the imaging results are mainly influenced by phase correlation. After substituting and rearranging we get the following

$$u_s(\varphi_\mathrm{a}, z_\mathrm{a}, \omega) = \iiint_{\boldsymbol{k}} \underbrace{\left[\iiint_{|\boldsymbol{r}_\mathrm{o}|<D} o(x_\mathrm{o}, y_\mathrm{o}, z_\mathrm{o}) e^{j(k_x x_\mathrm{o} + k_y y_\mathrm{o} + k_z z_\mathrm{o})} \,\mathrm{d}x_\mathrm{o}\,\mathrm{d}y_\mathrm{o}\,\mathrm{d}z_\mathrm{o} \right]}_{\mathcal{F}_{x_\mathrm{o}, y_\mathrm{o}, z_\mathrm{o}}} e^{-j(k_r \cos\Phi x_\mathrm{a} + k_r \sin\Phi y_\mathrm{a} + k_z z_\mathrm{a})} k_r \,\mathrm{d}k_r \,\mathrm{d}\Phi \,\mathrm{d}k_z$$

$$= \iint \underbrace{\left[\int O(k_x, k_y, k_z) e^{-jk_z x_\mathrm{a}} \,\mathrm{d}k_z \right]}_{\mathcal{F}_{k_z}{}^{-1}} e^{-j(k_r \cos\Phi x_\mathrm{a} + k_r \sin\Phi y_\mathrm{a})} k_r \,\mathrm{d}k_r \,\mathrm{d}\Phi \quad .$$

Taking the inverse Fourier transform with respect to k_z we get

$$u_s(\varphi_\mathrm{a}, k_z, \omega) = \iint O(k_x, k_y, k_z) e^{-j(k_r \cos\Phi x_\mathrm{a} + k_r \sin\Phi y_\mathrm{a})} k_r \,\mathrm{d}k_r \,\mathrm{d}\Phi$$

$$= \int \left[\int \underbrace{O(k_r, \Phi, k_z)}_{g(\Phi)} \cdot \underbrace{e^{-jk_r \rho_a \cos(\Phi - \varphi_\mathrm{a})}}_{f(\Phi - \varphi_\mathrm{a})} \,\mathrm{d}\Phi \right] k_r \,\mathrm{d}k_r = \int g(\varphi_\mathrm{a}) * f(\varphi_\mathrm{a}) k_r \,\mathrm{d}k_r$$

Taking the Fourier transform with respect to Φ we obtain

$$u_s(k_\Phi, k_z, \omega) = \int O(k_r, k_\Phi, k_z) \cdot \mathcal{F}_\Phi \left\{ e^{-jk_r \rho_a \cos\Phi} \right\} k_r \,\mathrm{d}k_r \tag{7}$$

Taking into account that only the values of the object spectrum lying on the Ewald sphere given by $4k^2 = {k_r}^2 + {k_z}^2$ contribute to the integral 7, the inversion gives the object function in cylindrical spectral coordinates

$$O(k_r, \varphi_\mathrm{a}, k_z) = \mathcal{F}_{k_\Phi}{}^{-1} \left\{ \frac{u_s(k_\Phi, k_z, \omega)}{\mathcal{F}_\Phi \left\{ e^{-jk_r \rho_a \cos\Phi} \right\}} \right\} \quad . \tag{8}$$

3.2 Stolt Mapping and Interpolation

The holographic data $u_s(\varphi_\mathrm{a}, z_\mathrm{a}, \omega)$ is scanned on an equidistant and linear grid with $\rho_\mathrm{a} = const$ with respect to the variables φ_a, z_a and ω. The inversion of the object function to cartesian coordinates can be only be done by 3D inverse Fast Fourier transform after it has been interpolated onto a Cartesian spectral grid (k_x, k_y, k_z). This operation is called Stolt-Mapping. The cartesian spectral grid is linked to the cylindrical spectral coordinates by

$$(k_x, k_y, k_z)^\top = (k_r \cos\varphi_\mathrm{a}, k_r \sin\varphi_\mathrm{a}, k_z)^\top = \left(\sqrt{4k^2 - {k_z}^2} \cos\varphi_\mathrm{a}, \sqrt{4k^2 - {k_z}^2} \sin\varphi_\mathrm{a}, kz \right)^\top \tag{9}$$

The interpolation is in our case realized by a so-called Gridding algorithm [6] or by using the results of Non Uniform Fourier Transform (NUFFT) theory [7].

3.3 Inversion Scheme

Finally we end up with the applied inversion scheme

$$o(x_\mathrm{o}, y_\mathrm{o}, z_\mathrm{o}) = \mathcal{F}_{k_x, k_y, k_z}{}^{-1} \left\{ \text{Stolt-Mapping} \left[\mathcal{F}_{k_\Phi}{}^{-1} \left\{ \frac{u_s(k_\Phi, k_z, \omega)}{\mathcal{F}_\Phi \left\{ e^{-jk_r \rho_a \cos\Phi} \right\}} \right\} \right] \right\} \quad . \tag{10}$$

4 EXPERIMENTAL RESULTS

4.1 Measurement Setup and Data Acquisition

The data acquisition was done with a Millimeter-Wave Linear Stepped Frequency Radar system (SFMCW) principally usable within the complete W waveguide band, i.e. 75 GHz ... 110 GHz. The cylindrical synthetic aperture was covered by sensor rotation about the z-axis and by a linear movement in the same direction. The TX power used was about 0 dBm. The frequency range was chosen to 90 GHz to 100 GHz including 201 frequency samples. These parameters lead to a range resolution of 1.5 cm and a range unambiguity of 3 m well suitable for the application.

The extent of the synthetic aperture was chosen to: $L_{z_\mathrm{a}} = 0.2\,\mathrm{m}$, with $n_{z_\mathrm{a}} = 101$ discretization steps and $L_{\varphi_\mathrm{a}} = 60\,^\circ$, with $n_{\varphi_\mathrm{a}} = 201$ angular increments as described by Fig. 1.

4.2 Imaging Results

The section shows exemplary results obtained with the SFMCW system and applying the imaging algorithm described previously. The application of the 3D cylindrical reconstruction algorithm described in (10) took about seven minutes on a conventional 2 GHz Pentium IV PC using MATLAB®. Most of the computation time was spent for the interpolation needed for the Stolt Mapping. Further dramatically improvements in computation time can be achieved by using precomputed interpolation matrices and switching to specialized computational hardware like DSPs or FPGAs.

Imaging a metallic gun Fig. 2 shows the setup and the images obtained for a metallic gun.

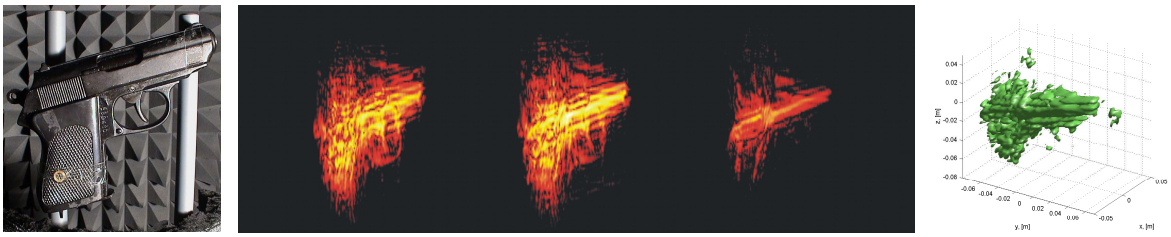

(a) photo of the object (b) Images of the gun (log.-scale 30 dB dynamic) at several depths (c) Iso-surface image

Fig. 2: metallic gun , not covered

Imaging a PVC torso packed with several items and covered with a pullover Fig. 3 shows the setup and the images obtained for a metallic gun.

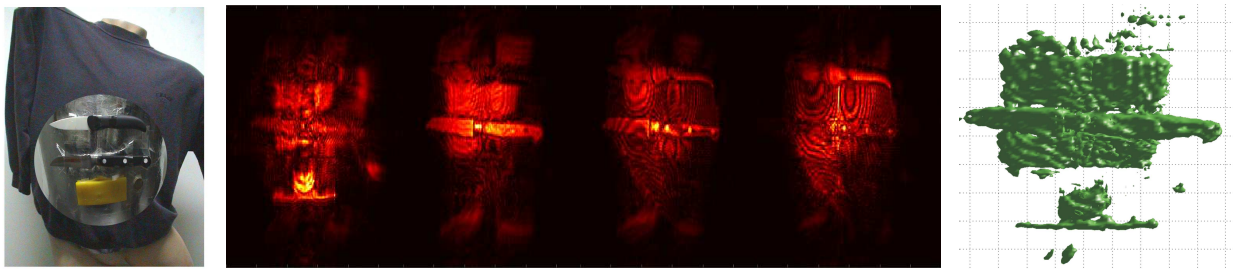

(a) photo of the object (b) Images of the dummy (linear scale) at several depths (c) Iso-surface image

Fig. 3: PVC dummy packed with a metallic knife, ceramic knife and a explosive simulant, everything covered with a pullover

The figures indicate that objects of interest can be imaged with resolution sufficient for identification even if hidden below some textile material. The data are principally suitable for 3D display but the display algorithms have still to be adopted for the proper indication of objects in front of the human body.

5 CONCLUSIONS

For the imaging of humans in a millimeter wave setup using SFMCW Radar inverse scattering reconstruction has been adapted to a cylindrical aperture geometry requiring a sequence of Fourier transforms. Reconstruction time takes still minutes but can be further improved by advanced interpolation and computational hardware techniques. Experimentally radar data on a cylindrical grid and processed by the 3D cylindrical reconstruction algorithm lead to suitable images also of hidden objects.

References

[1] D. M. Sheen, D. L. McMakin, H. D. Collins, Hall. T. E., and R. H. Severtsen. Concealed explosive detection on personnel using a wideband holographic millimeter-wave imaging system. *SPIE*, 2755:503 – 513, 1996.

[2] D. M. Sheen, D. L. McMakin, and T. E. Hall. Three-dimensional millimeter-wave imaging for concealed weapon detection. *IEEE Transactions on Microwave Theory and Techniques*, 49(9):1581–1592, September 2001.

[3] R. Bamler. *Mehrdimensionale lineare Systeme*. Nachrichtentechnik 20. Springer-Verlag, 1989.

[4] D. G. Dudley. *Mathematical Foundations for the Electromagnetic Theory*. The IEEE/OUP Series on Electromagnetic Wave Theory. IEEE Press, 1994.

[5] A. J. Devaney. Introduction to inverse scattering theory. Department of Electrical and Computer Engineering, Northeastern University, Boston, MA, Stanford Lectures, Lecture 1, Aug. 1999.

[6] F.T.A.W. Wajer, R. Lethmate, J.A.C van Osch, D. Graveron-Demilly, M. Fuderer, and D. van Ormondt. Interpolation from arbitrary to cartesian sample positions: Gridding. In *Proceedings of the ProRISC/IEEE workshop*, pages 571 – 577, Nov 30 - Dec 1st 2000.

[7] J. A. Fessler and B. P. Sutton. Nonuniform fast fourier transforms using min-max interpolation. *IEEE Transactions on Signal Processing*, 51(2):560 – 574, Feb. 2003.